Journal of Materials Chemistry C

Accepted Manuscript

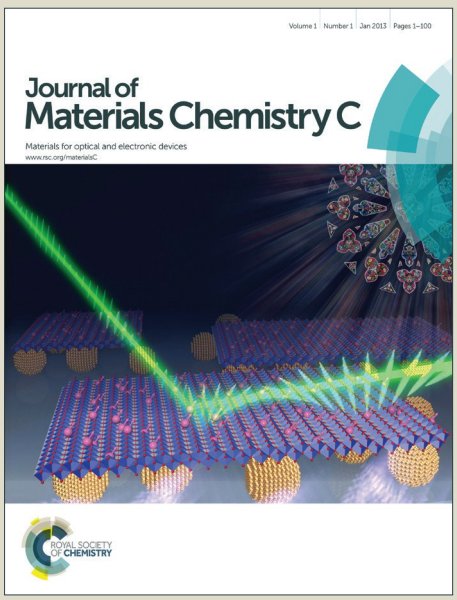

ROYAL SOCIETY OF CHEMISTRY

www.rsc.org/materialsC

Cite this: DOI: 10.1039/c0xx00000x

www.rsc.org/xxxxxx

ARTICLE TYPE

Optical Properties of SiO_2@M (M=Au, Pd, Pt) Core-shell Nanoparticles: Material Dependence, and Damping Mechanisms†

Xuemin Zhang,*[a] Shunsheng Ye,[b] Xun Zhang,[c] Lianpeng Wu[c]

Received (in XXX, XXX) Xth XXXXXXXXX 20XX, Accepted Xth XXXXXXXXX 20XX

DOI: 10.1039/b000000x

Optical properties of SiO_2@Pd and SiO_2@Pt core-shell nanoparticles (NPs) are investigated experimentally and theoretically, combined with a systematic comparison with that of traditionally investigated SiO_2@Au NPs. Theoretical calculations show that both plasmon hybridization effect and retardation effect affect the spectral peak position of all three kinds of core-shell NPs. These two effects compete with each other. The plasmon hybridization is a dominant influence in the case of a thinner shell, whereas the retardation effect becomes more important when the shell becomes thicker. As a result, the dipolar plasmon band reveals an initial blue shift and then red shift with the increase of shell thickness. Furthermore, the influences of core sizes and shell material on the competition are discussed. Finally, the relative strengths of absorption and scattering associated with the LSPR of three kinds of core-shell NPs are investigated. For SiO_2@Pd and SiO_2@Pt NPs, extinction is found to be dominated by absorption when shell thickness is less than ~20 nm, and a crossover from absorption dominance to scattering dominance takes place with the further increase of shell thickness. Contrarily, scattering is always the main decay process for SiO_2@Au NPs, which contribute more than 90% intensity of the extinction in despite of the shell thickness.

Introduction

Metallic nanoparticles (NPs) with typical dimensions of the wavelength of light and below will support fascinating optical resonances.[1] Particularly, localized surface plasmon resonance (LSPR), which essentially derived from spatially confined free electron oscillations that are resonant with incident photon frequency in noble-metal NPs and assemblies, is one of the most crucial ingredients in emerging new fields of nano-optics. A variety of promising applications have been found through extensively exploring the property of LSPR, including biosensing,[2] optical antennas,[3] plasmonic waveguides,[4] and surface enhanced spectroscopy (surface enhanced Raman scattering (SERS), surface enhanced infrared absorption, surface enhanced fluorescence and so on).[5]

The past decades have witnessed the rapid development of "plasmonics" into a vibrant sub-area of nanotechnology, and Au and Ag attract the most attention because these metals exhibit the favorable bulk dielectric properties. In contrast, optical properties of non-traditional plasmonic materials remain relatively unexplored, although it is gradually realized that tunable LSPRs can also be excited in some less favorable systems such as Pt, Pd and other kind of metals or even semiconductors.[6]

From the fundamental perspective, an important distinction between traditional plasmonic materials (Au and Ag) and non-traditional ones lies in their different LSPR decay process. It is long realized that a LSPR excitation predominantly decays through two ways, either decay radiatively (scattering, elastic channel) or via electron-hole pair formation (absorption, inelastic channel), and the ratio depends on the particle material, size and shape.[7] The radiative decay is dominate for Ag and Au particles with sizes over 20 nm to 40 nm, which has been recognized as a key factor for SERS application and biomedical imaging application. With respect to the inelastic channel, it involves hot electron-hole pair formation, and is closely related to the potential ability to utilize hot electrons (holes) for molecule decomposition or generation on the metallic surface.[8] Therefore, the inelastic decay channel is mostly concerned in applications such as photocatalysis and solar energy conversion to hydrogen.[9] From this point of view, catalytically active metals such as Pt or Pd are much more attractive. It is expected the combinations of intrinsic properties of Pt and Pd with the possibility to excite LSPR will give rise to new opportunities and challenges to the material science. As such, researches focused on the plasmonic property of Pt and Pd NPs are highly desirable.[10]

Core-shell NPs, consisting of metallic shells on dielectric cores, exhibit properties conspicuously different from their homogeneous counterparts. For instance, the plasmon resonance spectrum of metallic nanoshells can be tuned in a wide optical region by judiciously varying the shell thickness and/or core size.[11] The unique optical property promote metallic nanoshells a vibrant interest in nanoscience, promising for numerous technological applications including biosensing, photonic materials and surface enhanced spectroscopes.[12] However, few previous works have, so far, investigated the optical properties of

metallic core-shell NPs made from Pd and Pt, despite their importance in many catalytic reactions. Recently, Lee and co-workers have developed a simple route to synthesize SiO_2@Pd NPs. They provided a detailed characterization on the formation process of the Pd shell and catalytic property of obtained NPs, but optical property of SiO_2@Pd NPs were not discussed in their experiments.[13]

The aim of current work is to explore the LSPR property of SiO_2@Pd and SiO_2@Pt NPs, and give a systematic comparison between their optical properties and that of traditionally investigated SiO_2@Au NPs. Compared with previous chemically synthesized Pt and Pd NPs that always present SPR only in the UV and visible regions, clear and tunable plasmon bands in the near-infrared (NIR) region are visible for SiO_2@Pd and SiO_2@Pt NPs by judiciously varying the shell thickness. Furthermore, finite difference time domain (FDTD, Lumerical Solutions, Inc.) calculations are also applied. Theoretically, independent of the material of shell layer, the dipolar plasmon bands reveal initial blue shift and then red shift with the increase the shell thickness. At last, elastic/inelastic branching ratio of plasmon decay for different core-shell NPs are investigated. And our findings demonstrate interesting trends in the branching ratio both with regard to the shell thickness and material properties.

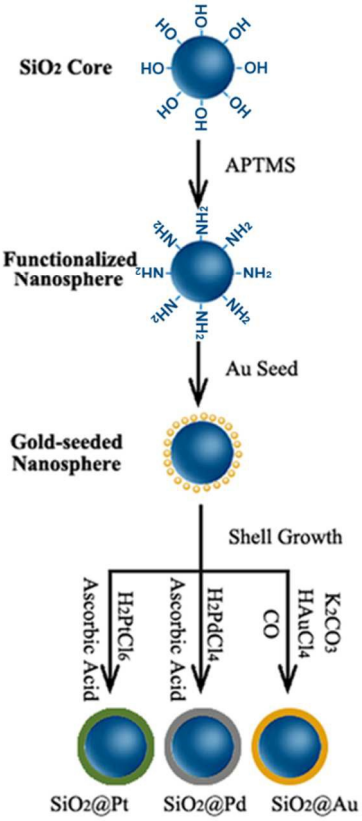

Figure 1. A schematic illustration of the procedures for the synthesis of SiO_2@M (M=Au, Pd and Pt) core-shell NPs.

Experimental Section

SiO_2@Au, SiO_2@Pd and SiO_2@Pt core-shell NPs were synthesized according to previous reports and a schematic illustration of the procedure was shown as Figure 1.[13, 14] Generally, the whole procedure can be divided into three steps, including functionalization of silica nanosphere with 3-aminopropyltrimethoxysilane (APTMS), modification of silica nanosphere with gold seeds and shell growth. These steps will be described in detail in the following.

Materials. All glassware used in the experiments were cleaned in aqua regia solution (3:1, HCl:HNO_3) followed by cleaning with piranha solution (7:3 concentrated H_2SO_4/30% H_2O_2), and then rinsed repeatedly with Milli-Q water (18.2 MΩ cm^{-1}). The silica colloidal spheres were prepared by the Stöber method,[15] and their average sizes were measured as 166 (±10) nm by SEM with a calibrated length. Tetrakis(hydroxymethyl) phosphonium chloride (THPC) and APTMS were obtained from Aldrich. Other chemical reagents were all used as received without any purification.

APTMS Functionalization of Silica Core. ~0.02 g silica nanosphere with diameter of ~166 nm was added into 40 mL ethanol, and then the suspension was ultrasonicated for at least 20 min to ensure the silica nanospheres uniformly dispersed. After that 200 μL APTMS was added into the suspension with continuous stirring overnight. Next, the mixture was boiled for 1 h, and then was left to cool to room temperature. Finally, the $-NH_2$ group functionalized core particles were washed at least five times in ethanol by centrifugation at 5000 rpm for 10 min, after which the functionalized nanospheres were redispersed in 1 mL ethanol.

Modification of Silica Core with Gold Seeds. A THPC gold solution composed of 1-2 nm Au colloid was firstly prepared according to Duff et al.[16] In short, 0.5 mL of 1 M NaOH was added to 47.5 mL of H_2O under rapid stirring, followed by the addition of 12 μL of aqueous THPC solution. After 5 min of continuous stirring, 2.06 mL of 1 wt% aqueous chloroauric acid was added in one quick motion, after which the solution immediately turned to a medium brown color. The final solution was refrigerated for at least 24 h before use.

To modify silica nanosphere with gold seeds, 1 mL APTMS functionalized silica nanosphere in ethanol was added into 25 mL gold seed solution, after which another 1.5 mL ethanol was also added. The existence of small amount of ethanol (less than 10 wt%) in the system is helpful for the attachment of gold seeds on the surface of $-NH_2$ functionalized nanospheres.[17] The mixture was stirred for 10 min and then was kept undisturbed at 4 □ for at least 24 h. Finally, gold-seeded silica nanospheres were washed at least five times in Milli-Q water by centrifugation at 5000 rpm for 10 min, after which the modified nanospheres were redispersed in 1 mL water and then stored at 4 □. The product has a shelf time of ~1 month.

Synthesis of Nanoshells. Gold nanoshells were synthesized through adding gold-seeded silica nanospheres into gold plating solution with CO as reducing agents. The gold plating solution was prepared by addition of 3.06 mL of 1 wt% chloroauric acid to 200 mL of 1.8 mM aqueous K_2CO_3. The solution was then stored at least for 24 h before use. CO rather than traditionally used H_2CO was chosen as reducing agents, for it can produce gold nanoshells with higher quality.[14] Reduction of Au^{3+} by CO was performed by aeration, with flow rate of ~25 sccm. Once CO was delivered into gold plating solution containing gold-seeded silica nanospheres, the solution will change from colorless to green in ~2 or 3 min, indicating the formation of SiO_2@Au NPs.

In order to make the reaction complete, CO was further delivered into the solution for ~5 min when the color did not chang any more.

As for Pd nanoshells, they were synthesized through adding gold-seeded silica nanospheres into H_2PdCl_4 solution with 10 mM L-ascorbic acid solution as reducing agents. H_2PdCl_4 solution was prepared by dissolving $PdCl_2$ (1 g) in a mixture of water (85 mL) and HCl solution (15 mL at 0.1 M). The as-prepared H_2PdCl_4 solution (56.4 mM) was used as a stock solution. In each experiment, 25 μL of gold-seeded silica nanosphere and certain amount H_2PdCl_4 stock solution were added into 15 mL of water at room temperature under vigorous stirring. After that, L-ascorbic acid solution (10 mM, a mild reducing agent) was added dropwise through a syringe controlled by a stepper motor, to reduce the palladium onto the core particles. With the addition of reducing agents, the color of the solution changed from original golden yellow into gray, indicating the formation of SiO_2@Pd NPs. The amount of ascorbic acid was kept 5 times as large as the amount of H_2PdCl_4, to make sure all the added H_2PdCl_4 can be reduced. For Pt shells, the synthesis procedure was similar as that of Pd shell. In short, they were synthesized through adding gold-seeded silica nanospheres into H_2PtCl_6 solution with 10 mM L-ascorbic acid solution as reducing agents. The reaction temperature was set as 80 ℃.

For all three kinds of nanoshells, the shell thickness was adjusted by controlling the ratio between the amount of gold-seeded silica core and the amount of plating solution. In all cases, the amount of gold-seeded silica core was kept as 25 μL, with the increase of gold plating solution from 10 mL to 60 mL, the shell thickness can be tuned in the range between 8 nm and 53 nm. Similar trends can be found in the synthesis of Pd and Pt nanoshells, their shell thickness can be tuned in the range of 13 nm to 80 nm and 13 nm to 65 nm, respectively. After the reaction was complete, the as-prepared nanoshells were washed at least 2 times in Milli-Q water by centrifugation at 1000 rpm for ~3 min, after which these NPs were redispersed in 5 mL water for further optical property measurements.

At last it should be noted the gold seeds have little influence on the optical properties of SiO_2@Pd and SiO_2@Pt core-shell NPs. According to Figure S1 in the ESI† and previous researches,[17] the surface coverage is only ~30% for 2 nm gold seeds on ATPMS-modified silica nanospheres. Therefore, the total Au content in the obtained Pd or Pt nanoshells (13 nm thickness) will be less than 2% and even fewer in thicker shells.

FDTD Calculations. We calculated the optical properties of the metallic nanoshells using the FDTD method (Lumerical Solutions, Inc.), the surrounding environment was set as water.

Characterization. Scanning electron microscopy (SEM) micrographs were taken with a Hitachi s-4800 field emission scanning electron microscope with primary electron energy of 15 kV. Transmission electron microscopy (TEM) was conducted using a JEM-2100 electron microscope at an acceleration voltage of 200 kV with a CCD camera. A Cary 5000 UV-vis-NIR spectrophotometer was used to measure the optical property of obtained nanoshell particles in the range of 400 nm to 1430 nm.

Results and Discussion

3.1 Synthesis of core-shell NPs with various shell thickness

Generally speaking, the formation of core-shell NPs is accomplished through metal deposition on the silica core with gold seeds as nucleation sites for shell growth. Meanwhile, the thickness of the shell can be adjusted by the proportion of gold-seeded silica cores to metal salt solution.

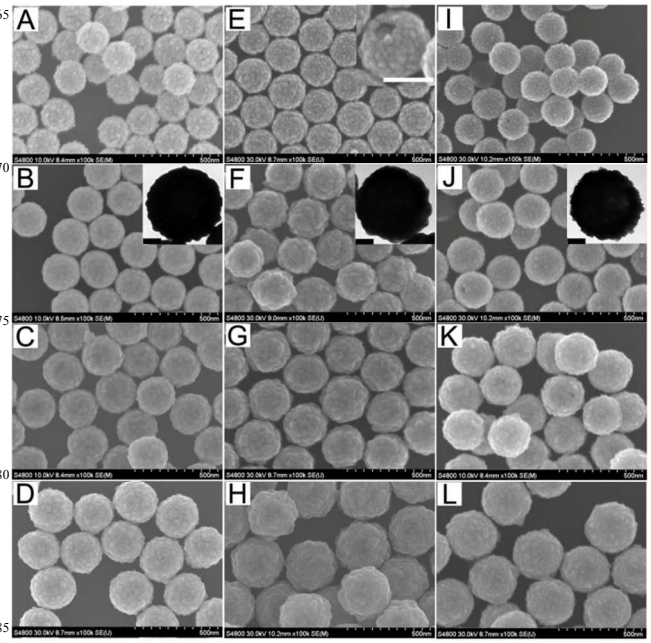

Figure 2. SEM images of SiO_2@Au (A-D), SiO_2@Pd (E-H) and SiO_2@Pt (I-L) core-shell NPs with various shell thickness. From A to D, the gold shell thicknesses are 8 nm, 23 nm, 37 nm and 53 nm, respectively. From E to H, the Pd shell thicknesses are 13 nm, 21 nm, 55 nm and 80 nm, respectively. From I to J the Pt shell thicknesses are 13 nm, 20 nm, 52 nm and 62 nm, respectively. Inset in E is a magnified image, with scale bar of 150 nm. Insets in B, F and J are TEM images of corresponding nanoparticles, with scale bar of 20 nm.

In this part, we will discuss the morphological features of as-prepared SiO_2@Au (2A-2D), SiO_2@Pd (2E-2H) and SiO_2@Pt (2I-2L) core-shell NPs (as shown in Figure 2). Revealed from these SEM images, no clear and definite morphological distinction exists between three kinds of core-shell NPs. In fact, they all exhibit relative rough surfaces, which are apparently different from bare silica cores that show clean and smooth surfaces (as shown in Figure S2), indicating the coating of metal shells onto silica cores. Besides, it is noted that the core-shell NPs generally have low poly-dispersities, implying the metals are uniformly deposited on each silica core. We further try to characterize the shell thickness through TEM measurement (as shown in insets in Figure 2B, 2F and 2J), however, the core/shell interface is undistinguishable. Therefore, we subtract the core diameter (~166 nm) from the average diameter of core-shell NPs to determine the shell thickness. Experimentally, the minimum shell thicknesses can be achieved are ~8 nm for Au shell, and ~13 nm for Pd and Pt shell. We should point out that the minimum shell thicknesses mentioned here just means the surface of silica cores are completely coated by metals. However, we are not sure whether the shell is continuous, or semi-continuous, or even just closely packed individual metallic NPs, for it is indeed not easy

to identify the details only through the SEM images (as shown in Figure S3 in the ESI).

3.2 Optical properties of SiO_2@Au NPs

The optical property of SiO_2@Au NPs will be first discussed, with an emphasis on their unique feature, or more specifically, the possibility of controlling the LSPR properties by the variation of the metallic shell thickness when holding the diameter of the dielectric core constant. It is expected the conclusions drawn in this section are helpful for further understanding the plasmonic property of Pd and Pt shell NPs.

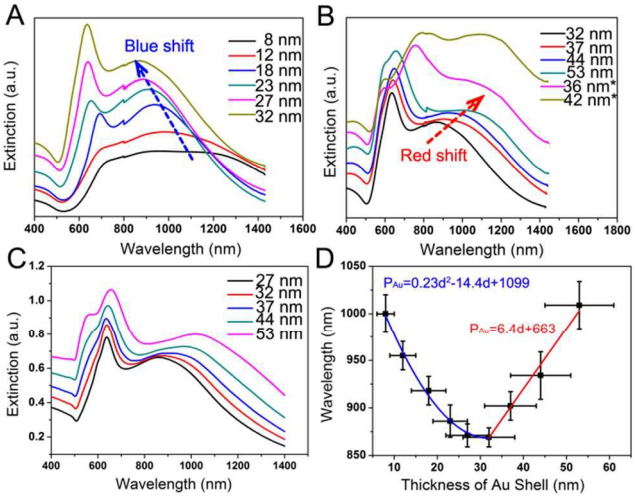

Figure 3. Extinction spectra of SiO_2@Au NPs with shell thickness varying from 8 nm to 32 nm (A), and 32 nm to 53 nm (B). Curves labeled with * in B indicate extinction spectra of SiO_2@Au NPs with much rougher surfaces. C, calculated extinction spectra of SiO_2@Au NPs with shell thickness varying from 27 nm to 53 nm. D, experimentally measured dipolar peak wavelength plotted with respect to the shell thicknesses.

For Au nanoshells with shell thickness from 8 nm to 32 nm, as shown in Figure 3A, an apparent blue shift of extinction peak from ~1000 nm to ~870 nm can be observed. This phenomenon can be explained using a plasmon hybridization theory developed by Nordlander and Halas group.[18] In addition to blue shift of extinction peak, these sequential extinction spectra increase in intensity, along with a band narrowing process. When the shell thickness reaches 18 nm, a much narrower quadrupole mode can be seen at the shorter wavelength range of broad dipolar plasmon band (~650 nm), and it becomes increasingly pronounced compared to the dipolar resonance.

With further increasing the shell thickness (32 nm-53 nm, as shown in Figure 3B), conversely, the extinction band in this stage experiences a red shift process. Simultaneously, the growing shoulder resulted from the octupole contribution gradually appears at ~580 nm. Figure 3C shows the FDTD calculated results. Because the blue shift process has been reported in many previous literatures, we show herein only the red shift process. Revealed from Figure 3C, the theoretical results are in good accordance with the experimental results.

It is noted that the red shift process of plasmon peak has been rarely reported and discussed before, for most previous researches focused on SiO_2@Au core-shell particles with relative thin shells, and theoretical calculations are generally based on the quasistatic and dipole approximations. However, in the case of larger core sizes or thicker shells, the quasi-static approximation is not justified due to significant phase-changes of the driving field over the particle volume. Or more exactly, the complicating effect of electromagnetic retardation appears, which arises due to a reduction of the depolarization field. The so-called retardation effect will result in the red shift of surface plasmon band.[19]

To give a more insightful understanding to the retardation effect, we investigated the dependence of optical property on the core sizes (as shown in Table S1 in the ESI). For NPs with core size of 40 nm, the extinction band blue shifts with the increase of shell thickness (from 8 nm to 20 nm). It is interesting to find that the peak position reaches a plateau of ~532 nm with further increase of the shell thickness (from 20 nm to 40 nm). No obvious red shift process can be found in this range, which indicates the retardation effect can be negleted for small NPs. However, if the shell thickness increases to 50 nm or thicker, i.e. the total size of the NP becomes large enough, one can also find the red shift process (the data is not shown). With respect to larger core sizes, such as 100 nm, 160 nm, 280 nm and 400 nm, no similar plateau can be seen. Red shift appears immediately after the bule shift process finishes, which is due to the enhancement of the retardation effect.

Based on the above discussion, the increase of shell thickness will give rise to two consequences. One is the decrease of the hybridization between the two fixed-frequency plasmon modes supported by the inner cavity and outer surface, leading to the blue shift of plasmon band.[18] The other consequence is the increase of particle size, making the retardation effect be more remarkable, which renders the red shift of plasmon band. These two effects competes with each other. According to Figure 3A and 3B, it can be concluded that the plasmon hybridization is a dominant influence in the case of a thinner shell, whereas the retardation effect becomes more important when the shell becomes thicker.

We further plot the experimentally measured dipolar peak position (P_{Au}) with respect to the shell thickness (d), shown as Figure 3D. After fitted, it is found that P_{Au} blue shifted quadratically with the increase of shell thickness in the first stage. A simple quadratic fit shows that $P_{Au}=1099-14.4d+0.23d^2$. By differentiating this relationship, we obtain the peak position sensitivity to the variation of shell thickness ($\delta P/\delta d$). $\delta P/\delta d$ can be considered as a parameter that evaluates the magnitude of dependence for P_{Au} on the plasmon hybridization effect. As such, sensitivity of -10.7 nm/nm at d=8 nm and 0 nm/nm at d=~31.3 nm are obtained. This result indicates the dependence of P_{Au} on d becomes weaker. When d exceeds 31.3 nm, a crossover from plasmon hybridization dominance to retardation effect dominance takes place. Hence, red shift of plasmon band is observed in the second stage. In contrary to the blue shifted process, the peak position red shifted linearly with the increase of shell thickness in the second stage, with a relationship of $P_{Au} = 663+6.4d$. And the slope 6.4 nm/nm represents the peak position sensitivity in this stage. Moreover, it is noted that this kind of liner relationship is very similar as previous reports focused on retardation effect for NPs of other morphologies, for examples, Ag nanodisks, Au nanocrescents and Au nanorods.[10, 20]

Experimentally, the maximum thickness of Au shell we can obtain is ~53 nm. Further increasing the gold plating solution

leads to the formation of SiO_2@Au NPs with a much rougher shell (as shown in Figure S4 in the ESI), and their extinction spectra (as shown in Figure 3B, labeled with *) are evidently different from those of above mentioned SiO_2@Au NPs. However, this part is not the interest of this paper.

3.3 Optical properties of SiO_2@Pd and SiO_2@Pt NPs

As for the SiO_2@Pd NPs, dipolar and higher order plasmon bands can also be observed (as shown in Figure 4A), with the former locating between 870 nm to 1400 nm and the latter in the shorter wavelength range (400 nm to 700 nm).

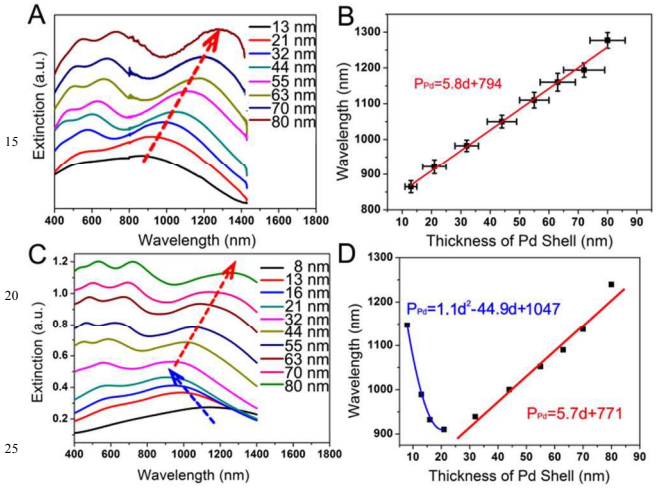

Figure 4. A, extinction spectra of SiO_2@Pd NPs with shell thickness varying from 13 nm to 80 nm. B, a liner fit of measured dipolar peak wavelength with respect to the Pd shell thicknesses. C, theoretically calculated extinction spectra of SiO_2@Pd NPs with shell thickness varying from 8 nm to 80 nm. D, calculated dipolar peak wavelength plotted with respect to the shell thicknesses.

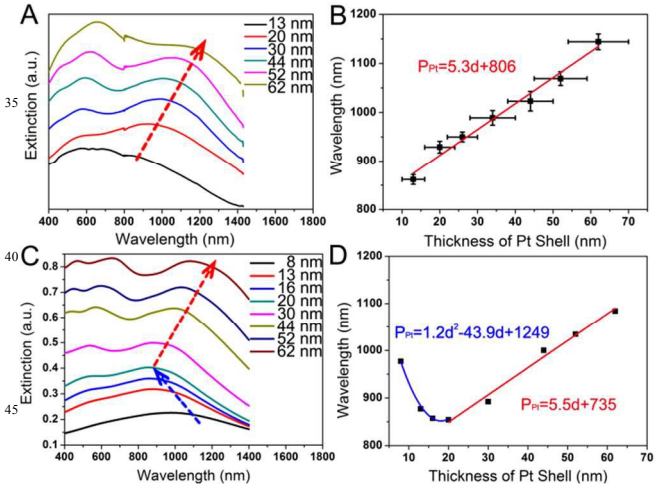

Figure 5. A, extinction spectra of SiO_2@Pt NPs with shell thickness varying from 13 nm to 62 nm. B, a liner fit of measured dipolar peak wavelength with respect to the Pt shell thicknesses. C, theoretically calculated extinction spectra of SiO_2@Pt NPs with shell thickness varying from 8 nm to 62 nm. D, calculated dipolar peak wavelength plotted with respect to the shell thicknesses.

An evident difference between the optical property of SiO_2@Pd NPs and that of SiO_2@Au NPs lies in the peak position response to the shell thickness. In fact, only red shift can be observed with the increase of Pd shell thickness from ~13 nm to ~80 nm. A liner fit is found for the dipolar peak position with respect to the shell thickness, that is P_{Pd}=794+5.8d (as shown in Figure 4B). This trend is similar as the second stage of SiO_2@Au NPs, so we attribute the linearly red shift to the retardation effect.

In the experiment, we have no difficulty in synthesizing SiO_2@Pd NPs with thicker shells. But when the shell thickness exceeds 80 nm, the plasmon peak will shift outside the spectrum window, in which region water will generate great noises. In contrast, how to synthesis SiO_2@Pd NPs with shell thickness less than 13 nm remains a big challenge. Currently, we can only obtain Pd nanoparticle decorated silica core rather than complete Pd shells when its thickness is less than 13 nm (see Figure S5). Therefore, we wonder whether blue shift of plasmon band with respect to the increase of shell thickness can be observed if the shell thickness is thin enough.

To verify this hypothesis, we resort to FDTD theoretical calculations, and the results are shown as Figure 4C. Starting with 8 nm Pd shell, we indeed observe a clear initial blue shift and then red shift process of the dipole mode plasmon band with respect to the increase of shell thickness. This result indicates that the plasmon hybridization effect do exist for SiO_2@Pd NPs. Taking advantage of theoretical results, a quadratic fit with P_{Pd}=1047-44.9d+1.1d^2 can be found in the blue shift process, while a liner fit with P_{Pd} = 771 +5.7d can be found in the red shift process. Comparing the theoretical results with experimental results, it is noted that they are generally in good accordance, except at the point of 13 nm shell thickness. We assume this discrepancy may be due to the morphological difference. In theoretical calculations, Pd shell is considered as smooth and continuous, but in fact its surface is very rough. Moreover, even with SEM images with higher magnification, it is still hard to identify whether the shell is continuous or just composed with a layer of densely packed Pd NPs (See Figure S3). Therefore, the experimental results may tend to represent the optical property of Pd NPs rather than that of a complete Pd shell.

We further investigate the optical property of SiO_2@Pt NPs, and it is interesting to find they share almost the same optical response as SiO_2@Pd NPs (as shown in Figure 5). The dipolar plasmon bands locates between 870 nm to 1400 nm, and higher order bands in the shorter wavelength range (500 nm to 700 nm, as shown in Figure 5A). Experimentally, only the red shift of dipolar plasmon band can be observed, and it follows a liner fit with P_{Pt} = 806 +5.3d (Figure 5B). In contrary, a clear initial blue shift and then red shift process is revealed when calculated using FDTD. Taking advantage of theoretical results, a quadratic fit with P_{Pt}=1249-43.9d+1.2d^2 can be found (d<20 nm), while a liner fit with P_{Pt} = 735 +5.5d can be found in the red shift process (d>20 nm, as shown in Figure 5C and 5D).

With these calculated results we can obtain peak position sensitivity of Pd and Pt nanoshells. Similar as SiO_2@Au NPs, in the first stage, the sensitivities decrease with the increase of shell thickness, implying that the dependence of peak position on the shell thickness becomes weaker, as shown in Figure 6. Besides, it is easy to calculate the crossover tickness (CT) from plasmon hybridization dominance to retardation effect dominance. The corresponding thickness are ~20.4 nm and ~18.3 nm for Pd and Pt nanoshells (when the silica core is 166 nm), respectively, which is much shorter than that of Au nanoshells (~31.3 nm).

Here, if we neglect the retardation effect in the first stage, CT means the point where plasmon hybridization between the inner cavity plasmon mode and outer surface plasmon mode vanishes. In other words, plasmon hybridization effect can be supported in thicker Au nanoshells than Pd and Pt nanoshells. Taking advantage of the theoretical calculations, we can also obtain CTs of the other sizes SiO_2@M NPs (as shown in Table S1-S3 in the ESI). For the investigated core sizes (40 nm, 100 nm, 160 nm, 280 nm and 400 nm), CT increases with the increase of core sizes, and more importantly, CT of SiO_2@Au NPs is always ~5 to 10 nm larger than that of SiO_2@Pd (and SiO_2@Pt) NPs of the same sizes.

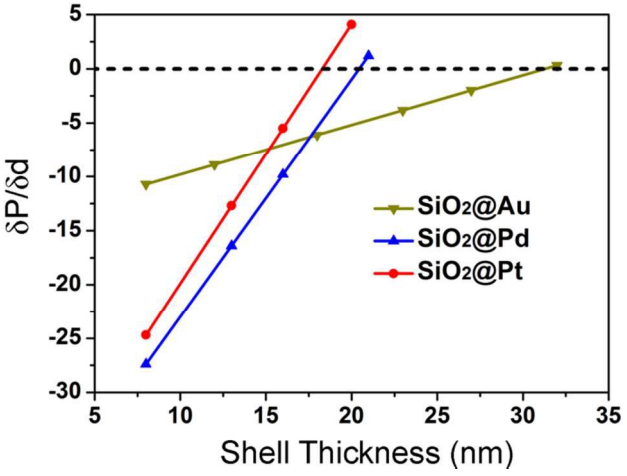

Figure 6. Plotted δP/δd with respect to the shell thickness for SiO_2@Pt (red), SiO_2@Pd (blue) and SiO_2@Au (dark yellow) core-shell NPs, respectively. Their intersection points with the reference line (δP/δd=0) indicate the switch threshold from plasmon hybridization dominance to retardation effect dominance.

In the meanwhile some recent reports have shown that the plasmon coupling between the cavity and sphere modes is similar to the decay of the plasmonic field in the interparticle gap of the particle-pair system.[21] In fact, we can also fit the blue-shift process in the first stage (in Figure 3-Figure 5) with a near-exponential curve:

$$P = P_0 + a^*\exp(-x/l) \quad (1)$$

where l indicates the decay length, yielding l=11.7 nm, 5.0 nm and 5.8 nm for Au, Pd and Pt nanoshells, respectively. Again, it is in consistent with the conclusion that plasmon hybridization effect can be supported in thicker Au nanoshells than Pd and Pt nanoshells.

This conclusion can be explained using the quasi-static approximation. The coupling strength is determined by the strength of the near-field **E**, or more specifically the polarizability **α** and the interparticle distance d. To facilitate the discussion we use the polarizability of spherical NPs to approximate **α** of nanoshells, which can be represented as the following equation:

$$\boldsymbol{\alpha} \propto 4\pi a^3 \frac{\varepsilon-\varepsilon_m}{\varepsilon+2\varepsilon_m} \quad (2)$$

where a is the radius of NP, and ε_m is the dielectric constant of the surrounding medium. ε is the complex dielectric function of metallic NPs, and it can be represent as:

$$\varepsilon=\varepsilon_r+\varepsilon_i \quad (3)$$

Combined with equation 2 and 3, it is apparent that **α** will experience a resonant enhancement under the condition that $|\varepsilon + 2\varepsilon_m|$ is a minimum. For classic plasmonic materials (such as Au and Ag) with $|\varepsilon_r|>>\varepsilon_i$ and $\varepsilon_i\approx0$, the resonance condition simplifies to $\varepsilon_r=-2\varepsilon_m$. But for Pt and Pd, they exhibit a higher value of the imaginary part of the dielectric function ε_i compared to Au (in the present spectral range, approximately 10 times larger).[22] That is to say, the magnitude of **α** of Pt and Pd nanoshells at resonance will be greatly reduced by the incomplete vanishing of its denominator. The larger polarizability **α** of Au nanoshlls leads to stronger near-field coupling, thus ensures the plasmon hybridization effect be supported in much thicker shell thickness than Pd and Pt nanoshells. In the end, it should be noted that the dipolar resonance condition in the quasistatic limit for core-shell NPs is much more complicated than that of spherical NPs,[21] however, we can also expect a similar conclusion (See equation S1 in ESI for details).

3.4 Absorption and scattering properties of SiO_2@Au, SiO_2@Pd and SiO_2@Pd core-shell NPs

At last, we investigated the relative strengths of elastic and inelastic processes associated with the LSPR of three kinds of core-shell particles. Figure 7 shows calculated extinction, absorption, and scattering intensity for SiO_2@Au NPs with shell thickness of 12 nm, 23 nm, 37 nm and 53 nm. In all cases, scattering dominated almost entirely the dipolar extinction (>90%), and the intensity of absorption dipolar peak decrease with increase of the shell thickness. When the shell thickness exceeds 37 nm, the dipolar absorption peaks almost disappear.

Figure 8 shows the corresponding data for Pd nanoshells, varying in shell thickness from 13 nm to 80 nm. In contrast to SiO_2@Au nanoparticle, extinction is found to be dominated by absorption for SiO_2@Pd nanoparticle with shell thickness of 13 nm. With increasing shell thickness, the scattering contribution to the total extinction efficiency becomes more and more significant, and a crossover from absorption dominance to scattering dominance takes place at shell thickness of 21 nm. When shell thickness reached 80 nm, scattering contributed ~75% of the total dipolar extinction.

As for SiO_2@Pt NPs, a similar optical property is found as SiO_2@Pd NPs (as shown in Figure 9). Again we notice a predominance of absorption for smaller shell thickness and a crossover to the scattering dominated region at shell thickness of ~20 nm. When shell thickness reaches 62 nm, scattering contributed ~75% of the total dipolar extinction.

This result is different from previous researches on optical property of Au, Pd and Pt NPs.[10] According to previous reports, the transformation from absorption dominance to scattering dominance have been observed for Au and Ag spherical NPs and nanodisks, while absorption is always found to dominate the dipolar extinction for Pt and Pd NPs. The difference between previous and current results is due to the morphology distinction between NPs, which is considered as an important factor in determining the plasmonic property of metallic NPs. However, in all these literatures, the branching ratio between absorption and scattering is always found to be larger for Pd and Pt NPs than

their Au counterparts of the same morphology. This phenomenon can also be traced to the higher value of ε_i of Pd and Pt compared to Au, which in turn derives from their significant interband activity. The origin of the fundamentally different dielectric response for these metals is eventually attributed to the differences in the electronic band structure. [22]

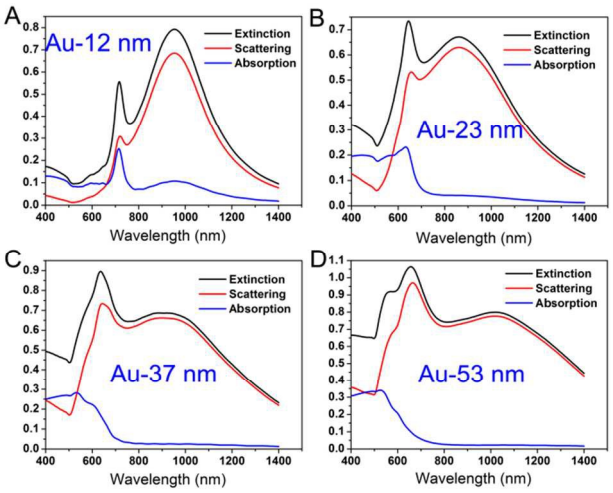

Figure 7. Calculated extinction (black), scattering (red), and absorption (blue) spectra for SiO_2@Au NPs with shell thickness of 12 nm (A), 23 nm (B), 37 nm (C) and 53 nm (D), respectively.

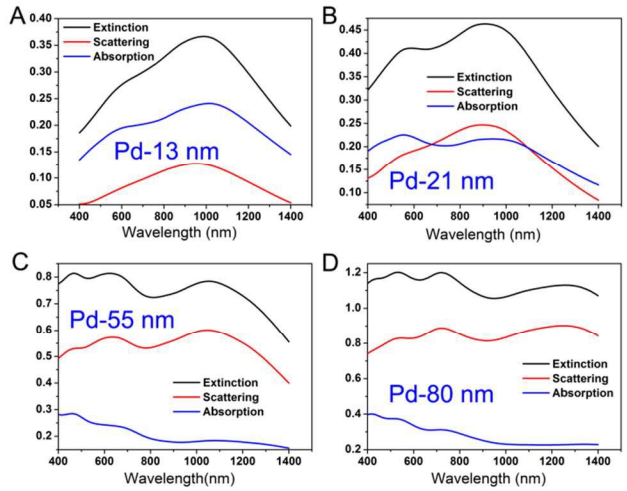

Figure 8. Calculated extinction (black), scattering (red), and absorption (blue) spectra for SiO_2@Pd NPs with shell thickness of 13 nm (A), 21 nm (B), 55 nm (C) and 80 nm (D), respectively.

Furthermore, it is interesting to find there is significant wavelength drift between the scattering and absorption bands in the calculated data (as shown in Figure 7 to Figure 9), with the maximum of the absorption peak always being at longer wavelength range of the scattering one. Careful observation of the spectra shows that the wavelength drift is significantly larger for Pt and Pd nanoshells (e.g., ~70 nm with shell thickness of 13 nm) compared to Au nanoshell (e.g., ~4 nm with shell thickness of 12 nm). Indeed, this phenomenon has been found in both previous experiments and calculations, and it is found that the deviation greatly depends on the particle size, shape and material, as well as the dielectric constant of surrounding environment.[23] Currently, the wavelength drift is believed to originate from the difference between the near-field (absorption) and far-field (scattering) optical responses of the core-shell NPs. However, to fully understand this effect, more theoretical and experimental works are necessary, which will be the subject of a future publication.

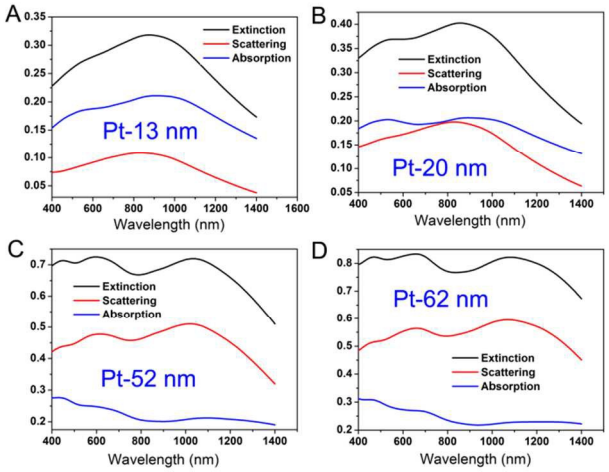

Figure 9. Calculated extinction (black), scattering (red), and absorption (blue) spectra for SiO_2@Pt NPs with shell thickness of 13 nm (A), 20 nm (B), 52 nm (C) and 62 nm (D), respectively.

Conclusions

In conclusion, we have succeeded in synthesis SiO_2@Au, SiO_2@Pd and SiO_2@Pt core-shell NPs with various shell thickness, and carried out a systematic experimental and theoretical research on the optical properties of these NPs. It is found both the plasmon hybridization effect and retardation effect influence the plasmon band position of three kinds of nanoshells, which results the dipolar plasmon band reveals an initial blue shift and then red shift with the increase of shell thickness. Dielectric constant is another important factor that affects the optical property of nanoshells. Due to the higher value of the imaginary part ε_i of Pd and Pt compared to Au, plasmon hybridization effect can be supported in much thicker Au nanoshells than Pd and Pt nanoshells. In the meanwhile, higher value of ε_i also leads to the branching ratio between absorption and scattering of Pd and Pt nanoshells be larger than their Au counterparts. For SiO_2@Pd and SiO_2@Pt NPs, extinction is found to be dominated by absorption when shell thickness is less than ~20 nm, and a crossover from absorption dominance to scattering dominance takes place with the further increase of shell thickness. Contrarily, scattering is always the main decay process for SiO_2@Au NPs, which contributes more than 90% intensity of the extinction in despite of the shell thickness.

Acknowledgements

The authors show their appreciation for the helpful discussion with Prof. Zhongqun Tian, Mr. Songyuan Ding and Jun Yi at Xiamen University. This work has been made possible by the financial support provided by the China Postdoctoral Science Foundation funded project (2012M521271) and China's General Administration of Quality Supervision, Inspection and Quarantine Bureau of Science and Technology Planning Project (2014IK135).

Notes and references

[a] *Department of Chemistry, College of Sciences, Northeastern University, Shenyang 110004, P. R. China, E-mail: zhangxuemin@mail.neu.edu.cn.*
[b] *State Key Lab of Supramolecular Structure and Materials, College of Chemistry, Jilin University, Changchun 130012, P. R. China..*
[c] *Jilin Entry-exit Inspection and Quarantine Bureau, Changchun 130062, P. R. China.*

† Electronic supplementary information (ESI) available: TEM image of gold-seeded silica cores; SEM images of bare silica nanospheres; magnified SEM images of SiO_2@Pd and SiO_2@Pt NPs with shell thickness of ~13 nm; SEM images of SiO_2@Au core-shell NPs with rough surfaces; Table S1-S3 which show the relationship between peak position, core sizes and shell thickness; Equation S1 which reveals the polarizability α of a metallic nanoshell. See DOI:10.1039/b000000x/

1 H. A. Atwater, *Sci. Am.*, 2007, **296**, 56; E. Ozbay, *Science*, 2006, **311**, 189; N. J. Halas, *Proc. Natl. Acad. Sci.* U. S. A., 2009, **106**, 3643; J. Henzie, J. Lee, M. H. Lee, W. Hasan and T. W. Odom, *Annu. Rev. Phys. Chem.*, 2009, **60**, 147.

2 M. E. Stewart, C. R. Anderton, L. B. Thompson, J. Maria, S. K. Gray, J. A. Rogers, R. G. Nuzzo, *Chem. Rev.* 2008, **108**, 494; A. Dmitriev, C. Hägglund, S. Chen, H. Fredriksson, T. Pakizeh, M. Käll, D. S. Sutherland, *Nano Lett.* 2008, **8**, 3893; X. Zhang, Z. Li, S. Ye, S. Wu, J. Zhang, L. Cui, A. Li, T. Wang, S. Li and B. Yang, J. Mater. Chem., 2012, **22**, 8903; Haes, A. J.; Van Duyne, R. P. *Anal. Bioanal. Chem.* **2004,** *379*, 920.

3 J. S. Shumaker-Parry, H. Rochholz, M. Kreiter, *Adv. Mater.* 2005, **17**, 2131; P. Muhlschlegel, H. J. Eisler, O. J. F. Martin, B. Hecht, D.W. Pohl, *Science* 2005, **308**, 1607; M. Navarro-Cia, S. A. Maier *ACS Nano* 2012, **6**, 3537.

4 J. P. Krenn, *Nat. Mater.* 2003, **2**, 210; J. P. Krenn, J. C. Weeber, E. Bourillot, J. P. Goudonnet, B. Schider, A. Leitner, F. R. Aussenegg, Ch. Girard, *Phys. Rev. Lett.* 1999, **82**, 2590; S. A. Maier, P. G. Kik, H. A. Atwater, S. Meltzer, E. Harel, B. E. Koel, A. A. G. Requicha, *Nat. Mater.* 2003, **2**, 229.

5 Z. Q Tian, B. Ren, J. F. Li, Z. L. Yang, *Chem. Comm.* 2007, 3514; P. Alonso-González1, P. Albella, M. Schnell, J. Chen, F. Huth, A. García-Etxarri, F. Casanova, F. Golmar, L. Arzubiaga, L. E. Hueso, J. Aizpurua, R. Hillenbrand, *Nat. Comm.* 2012, **3**, 684; F. Le, D. W. Brandl, Y. A. Urzhumov, H. Wang, J. Kundu, N. J. Halas, J. Aizpurua, P. Nordlander, *ACS Nano* 2008, **2**, 707; R. Bardhan, N. K. Grady, J. R. Cole, A. Joshi, N. J. Halas, *ACS Nano* 2009, **3**, 744.

6 E. M. Larsson, C. Langhammer, I. Zorić, B. Kasemo, *Science* 2009, **326**, 1091; C. Langhammer, I. Zorić, B. Kasemo, B. M. Clemens, *Nano Lett.* 2007, **7**, 3122; C. Langhammer, M. Schwind, B. Kasemo, I. Zorić, *Nano Lett.* 2008, **8**, 1461; M. Schwind, V. P. Zhdanov, I. Zorić, B. Kasemo, *Nano Lett.* 2010, **10**, 931; K. Manthiram, A. P. Alivisatos, *J. Am. Chem. Soc*. 2012, **134**, 3995; D. J. Rowe, J. S. Jeong, K. A. Mkhoyan, U. R. Kortshagen, *Nano Lett*. 2013, **13**, 1317.

7 C. F. Bohren，D. R. Huffman, *Absorption and Scattering of Light by Small Particles*, 1983, Wiley, New York; U. Kreibig, M. Vollmer, *Optical Properties of Metal Clusters*, 1995, Springer, Berlin.

8 V. P. Zhdanov, B. Kasemo, *J. Phys.: Condens. Matter* 2004, **16**, 7131.

9 Y. Tian, T. Tatsuma, *J. Am. Chem. Soc*. 2005, **127**, 7632; V. Subramanian, E. Wolf, P. V. Kamat, *J. Phys. Chem. B* 2001, **105**, 11439; A. Fujishima, K. Honda, *Nature* 1972, **238**, 37; M. Grätzel, *Nature* 2001, **414**, 338.

10 C. Langhammer, Z. Yuan, I. Zorić, B. Kasemo, *Nano Lett.* 2006, **6**, 833; C. Langhammer, B. Kasemo, I. Zorić, *J. Chem. Phys.* 2007, **126**, 194702; Y. Xiong, J. M. McLellan, J. Chen, Y.Yin, Z. Y. Li, Y. Xia, *J. Am. Chem. Soc.* 2005, **127**, 17118; Y. Xiong, J. Chen, B. Wiley, Y. Xia, Y. Yin, Z. Li, *Nano Lett.* 2005, **5**, 1237.

11 S. J. Oldenburg, R. D. Averitt, S. L. Westcott, N. J. Halas, *Chem. Phys. Lett.* 1998, **288**, 243; B. J. Jankiewicz, D. Jamiola, J. Choma, M. Jaroniec, *Adv. Colloid Interface Sci.* 2012, **170**, 28.

12 H. Wang, D. W. Brandl, F. Le, P. Nordlander, N.J. Halas, *Nano Lett.* 2006, **6**, 827; C. Graf, A. van Blaaderen, *Langmuir* 2002, **18**, 524; C. S. Levin, J. Kundu, A. Barhoumia, N. J. Halas, *Analyst*, 2009, **134**, 1745.

13 J. H. Kim, H. W. Chung, T. R. Lee, *Chem. Mater.* 2006, **18**, 4115; J. H. Kim, W. W. Bryan, H. W. Chung, C. Y. Park, A. J. Jacobson, T. R. Lee, *ACS Appl. Mater. Interface* 2009, 5, 1063; J. H. Kim, J. S. Park, H. W. Chung, B. W. Boote, T. R. Lee, *RSC Adv.* 2012, **2**, 3968.

14 B. E. Brinson, J. B. Lassiter, C. S. Levin, R. Bardhan, N. Mirin, N. J. Halas, *Langmuir*, 2008, **24**, 14166.

15 W. Stöber, A. Fink, E. Bohn, *J. Colloid Interface Sci.* 1968, **16**, 62.

16 D. G. Duff, A. Baiker, P. P. Edwards, *Langmuir* 1993, **9**, 2301.

17 S. L. Westcott, S. J. Oldenburg, T. R. Lee, N. J. Halas, *Langmuir* 1998, **14**, 5396.

18 P. Nordlander, C. Oubre, E. Prodan, K. Li, M. I. Stockman, *Nano Lett.* 2004, **4**, 899; E. Prodan, C. Radloff, N. J. Halas, P. Nordlander, *Science* 2003, **302**, 419.

19 M. Meier, A. Wokaun, *Opt. Lett.* 1983, **8**, 581.

20 R. Bukasov, J. S. Shumaker-Parry, *Nano Lett.* 2007, **7**, 1113; R. D. Near, S. C. Hayden, M. A. El-Sayed, *J. Phys. Chem. C*, 2013, **117**, 18653.

21 P. K. Jain, M. A. El-Sayed, *Nano Lett.* 2007, **7**, 2854; Bohren, F. Craig, Huffman, R. Donald, *Absorption and scattering of light by small particles*. John Wiley & Sons, Inc., New York, NY, 1983,first edition.

22 P. B. Johnson, R. W. Christy, *Phys. Rev. B* 1972, **6**, 4370; J. H. Weaver, *Phys. Rev. B* 1975, **11**, 1416; H. Ehrenreich, H. R. Philipp, *Phys. Rev.* 1962, **128**, 1622.

23 J. Zhu, J. Li, J. Zhao, *Appl. Phys. Lett.* 2011, **99**, 101901.

For Table of Contents Use Only

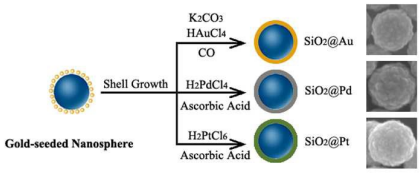

SiO_2@Au, SiO_2@Pd and SiO_2@Pt core-shell NPs are successfully synthesized, and a systematic investigation on their optical properties is carried out. It is found both the plasmon hybridization effect and retardation effect influence the plasmon band position, which results the dipolar plasmon band reveals an initial blue shift and then red shift with the increase of shell thickness. In the meanwhile, branching ratio between absorption and scattering of these nanoshells are shown.